Measurement of Dark Ice-Ablator Mix in Inertial Confinement Fusion

B. Bachmann et al.

Phys. Rev. Lett. **129**, 275001 — Published 29 December 2022

DOI: 10.1103/PhysRevLett.129.275001

Measurement of Dark Mix in Inertial Confinement Fusion

B. Bachmann,[1,*] S. A. MacLaren,[1] S. Bhandarkar,[1] T. Briggs,[1] D. Casey,[1] L. Divol,[1] T. Döppner,[1] D. Fittinghoff,[1] M. Freeman,[2] S. Haan,[1] G. N. Hall,[1] B. Hammel,[1] E. Hartouni,[1] N. Izumi,[1] V. Geppert-Kleinrath,[2] S. Khan,[1] B. Kozioziemski,[1] C. Krauland,[1] O. Landen,[1] D. Mariscal,[1] E. Marley,[1] L. Masse,[3] K. Meaney,[2] G. Mellos,[1] A. Moore,[1] A. Pak,[1] P. Patel,[1] M. Ratledge,[4] N. Rice,[4] M. Rubery,[1] J. Salmonson,[1] J. Sater,[1] D. Schlossberg,[1] M. Schneider,[1] V. A. Smalyuk,[1] C. Trosseille,[1] P. Volegov,[2] C. Weber,[1] G. J. Williams,[1] and A. Wray[1]

[1]*Lawrence Livermore National Laboratory, Livermore, CA 94551, USA*
[2]*Los Alamos National Laboratory, Los Alamos, NM, 87544, USA*
[3]*Commissariat à l'Energie Atomique, DAM, DIF, F-91297 Arpajon, France*
[4]*General Atomics, San Diego, CA 92121, USA*

(Dated: December 2, 2022)

We present measurements of ice-ablator mix at stagnation of inertially confined, cryogenically layered capsule implosions. An ice layer thickness scan with layers significantly thinner than utilized in ignition experiments enables us to investigate mix near the inner ablator interface. Our experiments reveal for the first time that the majority of atomically mixed ablator material is 'dark' mix. It is seeded by the ice-ablator interface instability and located in the relatively cooler, denser region of the fuel-assembly surrounding the fusion hotspot. The amount of dark mix is an important quantity as it is thought to affect both fusion fuel compression and burn propagation when it turns into hot mix as the burn-wave propagates through the initially colder fuel region surrounding an igniting hotspot. We demonstrate a significant reduction in ice-ablator mix in the hotspot boundary region when we increase the initial ice layer thickness.

Recent progress in laser indirect drive (LID) inertial confinement fusion (ICF) has advanced the field above the threshold of laboratory fusion ignition [1, 2]. These experiments make use of a high-Z hohlraum, typically made from gold or uranium, to convert the laser energy of the National Ignition Facility's 192 beams to a bath of x-rays that ablatively compress a capsule that is internally lined with heavy hydrogen (deuterium and tritium or DT) [3–7] . When the resulting fuel-ablator assembly stagnates, a hotspot is formed that reaches stellar core conditions and ideally initiates a nuclear fusion burn-wave that is driven by a chain reaction where alpha particles induce further DT reactions that produce more alpha particles and so on. Here, alpha particle stopping heats the surrounding cold and dense DT fuel which, step-by-step, becomes part of the igniting hotspot.

A key challenge for this process to happen efficiently is to keep the cold fuel layer clean of ablator material that would otherwise reduce stagnation compression and introduce a significant heat sink through radiation losses from the additional electrons supplied by the higher-Z ablator material [8]. The presence of fuel-ablator mix is currently hypothesized to be a major source of fusion performance degradation [9, 10] and becomes more relevant in the vicinity of ignition where the purpose of the cold fusion fuel is not only to confine the hotspot but feed the outgoing burn-wave. The origins of ice-ablator mix have been attributed to a variety of sources seeding instability growth at the ablation front [11, 12], inside the bulk ablator or at the various material interfaces present in ICF capsules [10]. Sources of instability growth include inhomogeneities and defects of the ablator material such as pits, voids and particles as well as engineering features such as the fill-tube [13–15] that is used to fill the capsule with fusion fuel, and the membrane [16] that centers and supports the capsule inside of the hohlraum. Other sources are the various interfaces at the ablation front, between doped and un-doped ablator layers and at the ice-ablator interface that can become unstable during the acceleration or deceleration phase of the implosion.

Understanding the impact of instability growth has been a decadal effort in ICF [17], mostly because of the convoluted nature of cause and effect, where often times instabilities seeded at one time and place manifest as observables at a later time and location so that pinpointing the impact of a specific degradation mechanism is challenging.

In this Letter we present a series of focused experiments to study and quantify the amount of deuterated carbon ablator material that is atomically mixed into the cold fuel. We find that from the total amount of mix (580^{+290}_{-190} ng, 13% of the hotspot mass) seeded by the ice-ablator interface, only 160 ± 20 ng are detected in the visible hotspot, leaving the rest (400^{+290}_{-170} ng) as 'dark' mix in the cold fuel region. This dark mix, which is located outside of the visible hotspot, has not been observed previously as mix measurements at stagnation of layered implosions have historically been limited to the x-ray emitting hotspot [9, 12, 18]. The presence of dark mix has, however, significant implications for the efficiency of fusion burn propagation in experiments near or above the ignition threshold. Indeed, we quantify the impact of increasing the initial ice layer thickness, resulting in more than a factor of two reduction in total mix mass reaching the hotspot periphery, increasing the clean fuel fraction which results in more efficient burn propagation.

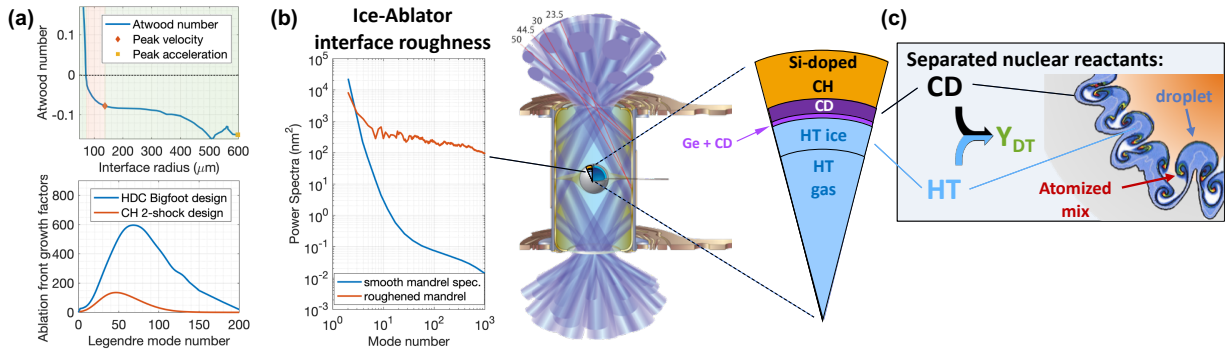

FIG. 1. (a) 2-shock implosion design showing stable Atwood number through peak-velocity and ablation front growth factors below. The ablation front growth is significantly lower than the similarly high-adiabat HDC Big-Foot implosion [19], which provides the 2-Shock platform's resistance to growth of the perturbation seeded by the capsule support tent. (b) Diagram of the hohlraum configuration with target capsule pie chart showing the separated nuclear reactants layers and artificially increased surface roughness at the ice-ablator interface. (c) Illustration of the atomized mix measurement at stagnation of the fuel-ablator assembly enabled by using separated nuclear reactants.

Simulations of the highest performing ICF implosions on the NIF include models for both hot mix into the hot spot at stagnation as well as dark mix from the fuel-ablator interface that does not reach the hot spot. However, without this additional dark mix, the simulations do not match the yield, down-scattered neutron ratio (DSR), ion temperature and hot spot size observed in the laboratory. Thus, the implementation and calibration of a model that accounts for the ice-ablator instability as described and enabled by the experiments presented in this paper, demonstrates the impact of this degradation mechanism by bridging the gap in simultaneously matching these measured fusion performance metrics. While x-ray imaging at stagnation provides direct evidence of hotspot mix, there has been no direct measurement of the dark mix until this work.

The experiments described here require a platform where both origins and seeds of ice-ablator mix can be prescribed in an otherwise hydrodynamically stable inertial confinement fusion design. The recently developed two-shock platform offers that via low ablation front growth and stable fuel-ablator Atwood number through peak velocity (see Fig. 1(a), where the Atwood number is defined as $(\rho_{ice}-\rho_{shell})/(\rho_{ice}+\rho_{shell})$) [20]. This platform uses a Si-doped CH ablator. Artificially roughening the inner ablator surface as shown in Fig. 1(b) to about 350 nm RMS, sets the seed for ice-ablator mix that grows principally in the deceleration phase when the interface becomes unstable (as seen in the red highlighted region at the top of Fig. 1(a)). The fuel-ablator mix caused by this seed is inferred to be equivalent to that produced in layered high-density carbon (HDC) implosions. This inference is made by using an identical model as described herein that reproduces the stagnation observables for recent, record yield, layered HDC implosions [2].

This setup allows us to focus on a single instability seed. To observe its impact, a key diagnostic to quantify

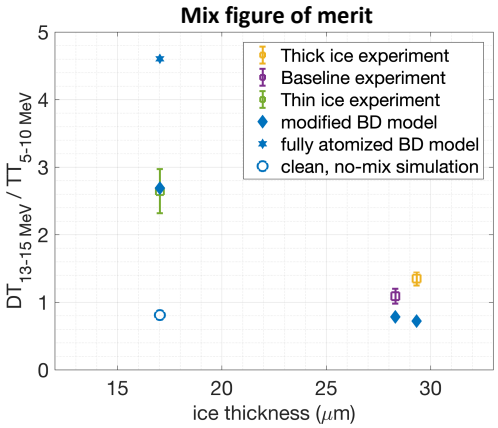

FIG. 2. Ratios of measured and simulated DT over TT neutron yields as a function of initial ice layer thickness showing a reduction in yield ratio when increasing the ice layer thickness from 17 μm to 29 μm.

the resulting ice-ablator mix at stagnation is a separated nuclear reactants measurement [21] that is implemented by doping the inner ablator layer with deuterium and using an HT fuel layer (Fig. 1(b)). During the implosion some of the deuterium mixes atomically with the tritium and reaches a critical density and temperature where nuclear DT reactions are initiated as shown in Fig. 1(c) and can be measured with the suite of neutron time-of-flight (nToF) detectors at the NIF.

Our mix figure of merit is the $DT_{13\text{-}15\ MeV}$ over $TT_{5\text{-}10\ MeV}$ yield ratio. Normalizing the separated nuclear reactants DT yield with the corresponding TT fusion yield that characterizes the hotspot performance allows us to compare individual experiments, as they exhibit typical shot-to-shot performance variations [22]. Increasing the initial ice layer thickness from 17 μm to 29 μm, resuls in a reduction of the yield ratio by a factor

of two from 2.7 ± 0.3 to 1.35 ± 0.1, as shown in Fig. 2. To establish a baseline, all the deuterium was removed from the ablator in a third experiment. In this third experiment the yield ratio reduced further to 1.09 ± 0.1, putting the yield ratio of the thicker ice layer close to, but significantly above, that baseline. DT reactions in the baseline experiment are a result of residual, <0.1% deuterium contamination in the HT fuel fill.

Fig. 2 also plots the ratios as computed by 1D radiation-hydrodynamic simulations of the three implosions. LASNEX [23] simulations of the three experiments employ a sub-grid model to dynamically include mixing at the fuel-ablator interface. This model employs a buoyancy-drag equation [24] to calculate Rayleigh-Taylor (RT) growth with the dimensionless values for the bubble alpha (0.06) and drag coefficient (2.5) adopted from the literature where the model was used to match classical mixing layer growth data [25]. Additionally, a Richtmeyer-Meshkov (RM) model saturates the growth of the RM instability below the transmitted shock speed due to the energy cost of the instability approaching supersonic growth [26]. For these simulations, the single dimensional input is the initial width of the mixing region at the fuel-ablator interface which was set at 350 nm based on the measured roughness of the mandrels on which the capsules were coated shown in Fig. 1(b). By default the model would assume that the material within the layer width evolved by the above RT and RM sources is atomically mixed; however, this is inconsistent with recent theories of mixing that require a minimum state for the development of fully turbulent mixing [27, 28]. Therefore, each computational zone can be subdivided yielding a free model parameter that can be used to adjust the sub-volume fraction of atomized mix. This free parameter is then calibrated to match the measured DT/TT yield ratio shown in Fig. 2. A more detailed description of this model can be found in Appendix (A). Using this model we infer that approximately 40% of the mix layer volume is allocated to atomic mix of ice-ablator material at stagnation.

To gain a deeper understanding of where the ice-ablator mix is located, we can measure the apparent ion temperature (T_{ion}^{app}) [29] of the deuterium and tritium ions that underwent DT fusion (see Appendix (B) for details). In addition we can calculate the average electron temperature of the hotspot [13, 30]. This is done by differentially filtering the x-ray emission in the energy range where both x-ray and neutron production approximately scale with the same power of temperature [31]. The results are shown in Fig. 3. Here the x-ray inferred electron temperatures range from 3.3 to 4.0 keV, while T_{ion}^{app} is 2.2 ± 0.24 keV for the two experiments that use the deuterium doped ablator. This significant reduction of temperature versus the hotspot temperature shows that the DT reactions are predominantly occurring in the much colder ice-vapor region. This is confirmed by

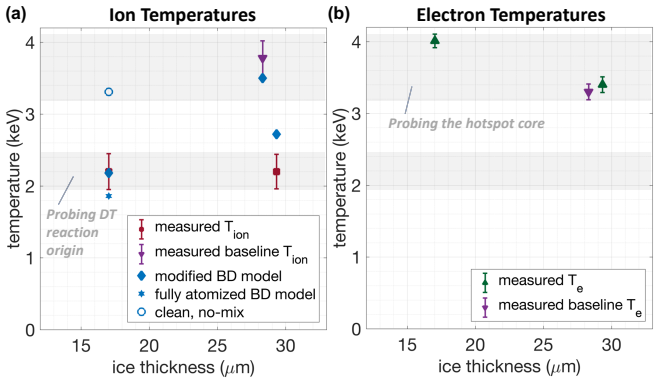

FIG. 3. (a) Measured and simulated Ion temperatures as a function of initial ice layer thickness. The measurements are derived from neutron time-of-flight detectors and probe the regions where the DT reactions originate, which occur predominantly in the cooler ice-ablator mix region. (b) Measured hotspot electron temperatures using differentially filtered x-ray penumbral images.

removing the deuterium from the ablator in the baseline experiment, resulting in $T_{ion}^{app} = 3.8 \pm 0.25$ keV, which is again in the range of the inferred hotspot electron temperatures. Shown in Fig. 3(a) are also corresponding simulation results using the new buoyancy-drag mix model that is calibrated by the DT/TT yield ratio.

We can also estimate the absolute amount of CD mix mass m_{CD} in the ice-ablator mix region by solving the nuclear yield equations of both TT and DT neutron production for the product of density and volume of the DT reaction region, given by Eq. (7) in Ref. [32], detailed in Appendix (C). Monte Carlo sampling the known constituents of these equations, by randomly drawing from their individual uncertainty distributions provides an estimate of the probability density functions (PDF) of the CD mix mass and tritium number densities for the DT and TT reaction regions, as well as of the hotspot core mass, pressure and density. The results for the CD mix mass and corresponding mix mass fraction are shown in Fig. 4(a) and show a significant decrease in CD mix mass near the hotspot boundary when increasing the ice layer thickness from 17 to 29 μm. This reduction in observed mix mass can be interpreted in two ways. First, by systematically varying the ice layer thickness we can effectively probe how much ablator material mixed into different ice layer depths of an equivalent full layer thickness ignition capsule. Second, this burn-weighted mix mass is a subset of the total mix mass that can play a role in reducing fuel compression at stagnation. It can also adversely affect burn propagation when it turns into hot mix as the burn-wave propagates through the initially cold, mix contaminated, ice layer surrounding an igniting hotspot.

We can also calculate the x-ray mix enhancement factor from the hotspot, which is the factor of x-ray emission

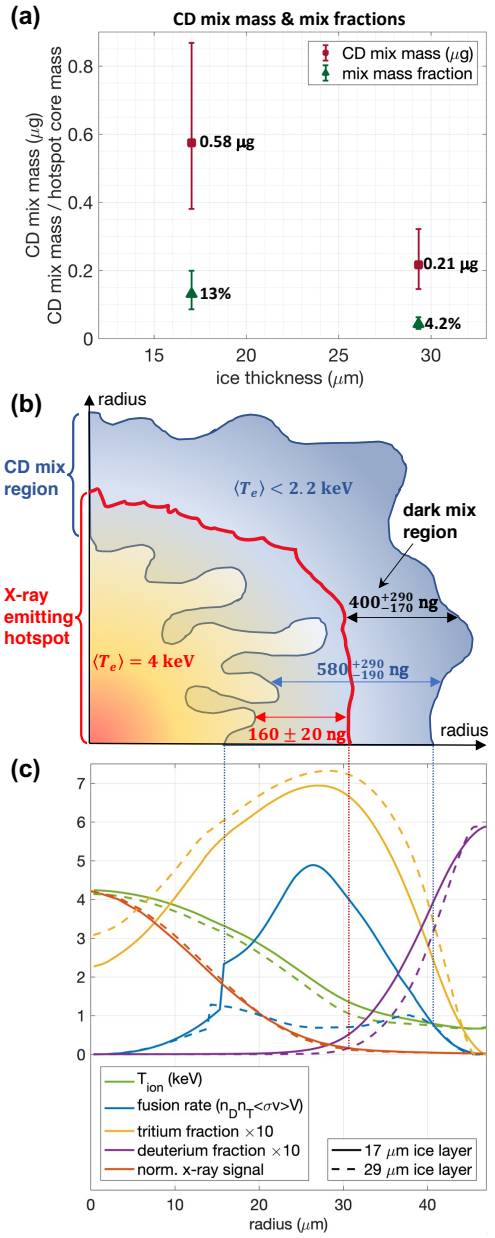

FIG. 4. (a) Experimentally inferred CD mix masses and mix fractions as a function of initial ice layer thickness. (b) Illustration of CD mix region comprised of dark mix and hotspot mix regions showing the majority of ablator material is dark mix. (c) Lasnex simulations using the modified buoyancy-drag mix model showing the fuel ablator assembly at peak burn. Shown are ion temperatures, normalized DT fusion rates, the atomic D and T fractions and the normalized detected x-ray signals as a function of radius for both initial ice layer thicknesses.

that is in excess of what is expected from a pure hydrogen plasma and a result of higher Z material, or mix, that is present in the hotspot. When CD mix enters the hotspot the total energy emitted by x-rays is elevated in comparison to what a hotspot would emit without mix but producing the same amount of TT reactions. The latter can be derived from the ratio of x-ray over neutron production given by Eq. (4) in Ref. [12] and is detailed in Appendix (D). The resulting x-ray enhancement is 1.24 ± 0.03 and the x-ray emitting mix mass yields $m_{CD(Ge)} = 160 \pm 20$ ng.

The x-ray enhancement measurement and the separated nuclear reactants measurement can be combined by subtracting the mix mass PDF of the hotspot from the total CD mix mass PDF inferred with the separated nuclear reactants measurements. This results in a remaining mix mass of 400^{+290}_{-170} ng, which presents itself as 'dark' mix, or mix that is located outside, but close to the boundary of the x-ray emitting hotspot as shown in Fig. 4(b). This evidence for dark mix is further supported by spectroscopic measurements of the hotspot. Here we used the NIF X-ray Spectrometer (NXS at $10.5-15$ keV) [34] and the Imaging and Spectroscopy Snout (ISS at 8 – 12.5 keV) [35] to capture any germanium line emission that would originate from Ge mixing from the inner ablator layer into the hotspot. Neither the thicker, nor the thinner ice layer experiment showed evidence of Ge line emission, supporting the observation that the majority of mix is located outside of the x-ray emitting hotspot. We estimate the NXS detection threshold for Ge He-beta line-emission, which would be spectrally separated from any hohlraum Au L-shell emission, to be around 6 ng of Ge, based on atomic kinetics simulations capturing the range of expected hotspot boundary conditions. Given our inferred hotspot mix mass of $m_{CD(Ge)} = 160 \pm 20$ ng, and 0.2% Ge atomic dopant fraction in the innermost 1 μm ablator, we estimate $0.6-4$ ng Ge to be co-located with CD mix in the x-ray emitting hotspot periphery. As a result, the absence of visible Ge line emission sets an upper limit for the hotspot mix that is consistent with the amount derived using the x-ray enhancement factor and thus provides further evidence for the observation of dark mix.

The modified buoyancy-drag model yields 560 ng of CD mass mixed into the hotspot periphery, which is consistent with our observation of 580^{+290}_{-190} ng and shows radial profiles of DT fusion rates and x-ray emission that are consistent with our dark mix observation (see Fig. 4(c)). The model has subsequently been applied to 1D Lasnex simulations of recent burning plasma implosions on the NIF that use a crystalline high density C ablator [1, 2]. In these implosions, the fuel-ablator interface has not been deliberately roughened and is therefore much smoother; however, other seeds for mixing such as inhomogeneities and defects in the ablator material have been identified. While the seeds of instability occur randomly in the HDC ablator as opposed to the prescribed seed in this work, we expect the mix model once calibrated to the prescribed CH case to be accurate for the interpenetration of fuel and ablator in the HDC case. This is because the behavior of bubble and spike growth beyond the linear regime

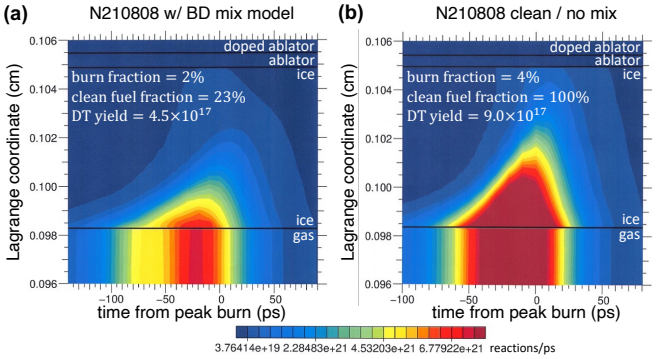

FIG. 5. LASNEX simulations of the first NIF shot to exceed the Lawson criterion for Ignition. (a) Simulations using the modified buoyancy-drag mix model show how burn propagation is quenched by initially dark mix, producing a total burn fraction of 2% and a clean fuel fraction of 23%, in comparison to (b), a clean, no-mix simulation of the same experiment.

depends on the plasma viscosity and mass diffusivity of the constituent materials, which are similar for carbon and CH [27]. The 1D BD simulations can reproduce the stagnation observables of these high-performing layered implosions when the width of the mixing region is initialized between 300-450 nm and all of the other (dimensionless) parameters including the surface-to-volume ratio are held fixed at the values used to match the data reported in this manuscript. Thus one can infer for these burning plasma implosions a similar behavior for the fuel-ablator mix that includes a majority of the mix mass remaining in the fuel as dark mix at the edges of the hot spot at and before stagnation. The impact of this ice-ablator mix can be seen in Fig. 5, comparing the burn propagation in simulations of the first NIF shot (N210808), which exceeded the Lawson criterion for ignition [2]. Here we compare a clean, no-mix simulation to a simulation that makes use of the modified buoyancy-drag mix model, where initially dark mix effectively quenches burn propagation.

In summary, we have conducted a series of experiments to study ice-ablator mix at stagnation of cryogenically layered ICF capsule implosions. Using a separated nuclear reactants technique in combination with differentially filtered hotspot x-ray imaging, we quantify the amount and thermophysical conditions of atomized ice-ablator mix. We observe dark mix that makes up $9.2^{+6.7}_{-3.8}\%$ of the hotspot mass and experiences thermal temperatures of less than 2.2 keV. This dark mix is located in the ice-vapor region surrounding the hotspot and constitutes $2.5^{+2.0}_{-1.1}\times$ the amount of mix visible in the hotspot. Knowing the amount of dark mix in the hotspot periphery is especially crucial for implosions close or above the ignition threshold, where this dark mix will limit compression and turn into hot mix as the burn-wave propagates through the initially cold ice layer surrounding an igniting hotspot. Measuring this dark mix enables calibration of novel mix models that will allow predictions for high-yield DT experiments and help our understanding and mitigation of ice-ablator mix. For example, increasing the ice layer thickness resulted in a $> 2\times$ reduction of the total mix mass in the hotspot periphery region that will eventually be consumed by the fusion burn wave, demonstrating a promising lever to achieve more efficient burn propagation.

ACKNOWLEDGEMENT

This work was performed under the auspices of the U.S. Department of Energy by Lawrence Livermore National Laboratory under Contract DE-AC52-07NA27344 [38].

APPENDIX (A) DESCRIBING THE MODIFIED BUOYANCY-DRAG MIX MODEL

The LASNEX [23] simulations of the three experiments employ the modified buoyancy-drag model described in the text, with the initial mixing layer dimension determined by the measured interface roughness and the mode number chosen to be 200 based on separate calculations of growth factors for the fuel-ablator interface; simulations later confirmed the amount of mixing was roughly independent of mode number above mode 175. With these constraints on the model, a simulation that assumes the mixing layer is completely atomically mixed such that all the D in the ablator material in the layer is available to react with all of the T in the fuel material calculates a DT/TT ratio of 4.6, indicated by the star in Fig. 2. Therefore, an additional degree of freedom must be added to the model to achieve a better match to the measured ratio. In particular, the assumption of a completely atomically mixed layer at stagnation is inconsistent with theories of hydrodynamic mixing that reduce classical RM and RT growth rates and predict a minimum state necessary for transition to turbulence [27, 28]. Therefore, we make use of a capability within the LASNEX model that permits only a sub-volume of each computational cell to contain atomically mixed material, while the remaining sub-volumes consist of the pure material "droplets" from either side of the mixing interface. This extra degree of freedom is illustrated schematically in Fig. 6(a), showing a mixing layer with boundaries evolving in time in accordance with the RM and RT sources of the dynamic mix model. The added degree of freedom for the mix model then takes the form of the evolution of the atomically mixed volume, which limits the amount of D and T within the mixing layer that is available to react. Within the code, this additional degree of control on the size of the atomic mix sub-volume is done by a surface-to-volume (AOV) multiplier that acts to control the average size of the droplets of pure material

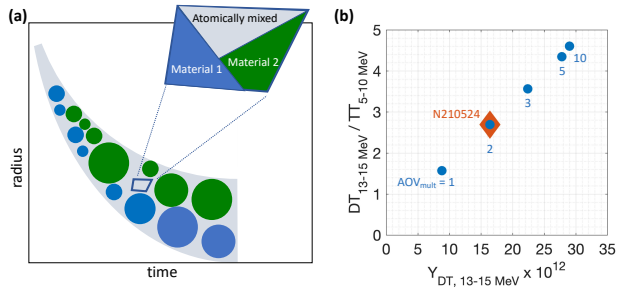

FIG. 6. (a) Schematic illustrating the capability of the buoyancy-drag (BD) mix model to evolve in each computational zone as a function of time volume fractions of both the pure ablator and ice materials as well as a volume fraction of atomically mixed material. (b) Nuclear yield ratios as a function of total DT yield for a range of droplet surface-to-volume ratios fitting the data for an atomically mixed volume fraction of $\sim 40\%$.

within the layer. Fig. 6(b) illustrates the effect of changing this multiplier on the absolute DT yield and DT/TT ratio calculated by the simulation. For these simulations, an AOV multiplier ≥ 10 results in completely atomized mixing in the layer, both in terms of the fraction of each cell that is allocated to atomically mixed material as well as the DT yield and DT/TT ratios calculated to be those for 100% atomic mixing. From Fig. 6(b), we find that an AOV multiplier of 2 represents a good fit to the observed mixing signal. This value represents approximately 40% of the cell volumes within the mixing layer at stagnation allocated to atomic mix of the ablator and fuel materials.

APPENDIX (B) ON OBSERVED ION TEMPERATURES

The apparent ion temperature $\mathrm{T}_{\mathrm{ion}}^{\mathrm{app}}$ is commonly measured by the doppler broadening of the nToF traces that are a result of DT reactions. Note that these distributions can be further broadened due to residual kinetic energy and therefore provide an upper limit for the average ion temperature [36]. Since electrons and ions are in local thermodynamic equilibrium at these conditions, this measurement provides an upper limit for the thermal temperature of the regions where the DT reactions originate. Further, $\mathrm{T}_{\mathrm{ion}}^{\mathrm{app}}$ also provides an upper limit for the thermal temperature of the mix region: In addition to residual kinetic energy increasing $\mathrm{T}_{\mathrm{ion}}^{\mathrm{app}}$, it will also be weighted by DT reactions that originate in the much hotter fusion hotspot due to the deuterium contamination of the HT fuel. Therefore, when averaging, this reduces the weighting of the cooler mix region temperature.

While the DT/TT ratio shown in Fig. 2 decreases dramatically when the initial ice layer thickness increases, $\mathrm{T}_{\mathrm{ion}}^{\mathrm{app}}$ is similar for the two experiments containing deuterium doped ablators. This is because the reaction region is largely set by the temperature where mix is present. Then the measured apparent DT ion temperature is a result of the mixing and subsequently reacting deuterium and tritium ions. Increasing the ice layer thickness increases the thickness of the boundary layer in between pure ablator material and hotspot. Therefore, less mix propagates to the regions that are close enough to the hotspot to get hot enough to create DT reactions, reducing the DT yield, but not necessarily affecting the apparent DT ion temperature. Because the hotspot temperature profile is for the most part determined by conversion of the implosion kinetic energy into internal energy at stagnation, the temperature profile is similar for both implosions. In the thinner ice case, however, the fuel at the edge of the hot spot will contain a larger fraction of deuterium due to the proximity to the mixing interface. Thus, for the two implosions the apparent DT ion temperature can be similar while the DT/TT ratio will be greater for the thinner ice case.

APPENDIX (C) ON MIX MASS CALCULATION FROM SEPARATED NUCLEAR REACTANTS

The absolute amount of CD mix mass m_{CD} in the ice-ablator mix region can be calculated by solving the nuclear yield equations of both TT neutron production ($Y_{TT-n} \approx 2\frac{1}{2}\, n_{T,1}^2 \langle\sigma v\rangle_{TT}\, V_1\, t$) and DT neutron production ($Y_{DT} \approx n_{D,2}\, n_{T,2}\, \langle\sigma v\rangle_{DT}\, V_2\, t$) for the product of density and volume $n_{D,2}\, V_2$ of the DT reaction region (index 2) and for the density of the TT reaction region (index 1) $n_{T,1}$, given by Eq. (7) in Ref. [32], where

$$m_{CD} = n_{D,2}\, V_2\, (A_{r,D} + \frac{A_{r,C}}{1.5})\, u, \tag{1}$$

$$n_{D,2}\, V_2 \approx \frac{Y_{DT}}{n_{T,2}\, \langle\sigma v\rangle_{DT}\, t}, \tag{2}$$

$$n_{T,2} \approx n_{T,1} \frac{T_1}{T_2} \text{ and } n_{T,1} \approx \sqrt{\frac{Y_{TT-n}}{\langle\sigma v\rangle_{TT}\, V_1\, t}}. \tag{3}$$

Here, $A_{r,D}$ and $A_{r,C}$ are the atomic weights of deuterium and carbon, u is the nucleon mass and $\langle\sigma v\rangle$, V, T are the reactivities, volumes and temperatures of the DT and TT reaction regions and t is the burn duration. As described in Ref. [32] we also assume that these two regions are experiencing the same pressure and that the additional pressure caused by the CD mix is negligible, which effectively provides a lower limit for the CD mix mass.

APPENDIX (D) ON HOTSPOT MIX MASS CALCULATION

The total x-ray energy emitted from a hotspot that produces the same amount of TT reactions as we measured here, but without any ablator mix contained within

the hotspot can be derived from the ratio of x-ray over neutron production given by Eq. (4) in Ref. [12], where we adjusted for TT reactions from a H:T = 1:3 hydrogenic fuel mixture and using a more recent fit to the emission coefficients of the DCA [37] opacity tables:

$$\frac{X_{\nu,HT}}{Y_{TT}} \approx 6.91 \times 10^{-32} \frac{4\pi}{\langle\sigma v\rangle_{TT}} \frac{1}{T_1^{0.15}} \frac{e^{-h\nu/kT_1}}{(h\nu)_{keV}^{0.39}} \,(\mathrm{J/keV}). \tag{4}$$

The resulting mix enhancement factor (or the amount of excess x-ray emission due to mix) is then given by $X_{enh} = X_{\nu,emit}/X_{\nu,HT}$, where the emitted x-ray energy $X_{\nu,emit}$ can be inferred from the x-ray penumbral imaging data [13, 33]. The resulting x-ray enhancement is 1.24 ± 0.03 and can subsequently be solved to yield the atomic ratios of all mixed species k with $X_{enh} = (1 + \sum_k x_k Z_k)(1 + \sum_k x_k Z_k^2)$, where $x_k = n_k/(n_T + n_H)$ and Z_k are the atomic ratio and atomic number. The x-ray emitting mix mass yields $m_{CD(Ge)} = m_{TH} \sum_k (x_k A_k) \,/\, A_{TH} = 160 \pm 20\,\mathrm{ng}$, where A_k is the atomic mass number. We note that even if only a portion of the hotspot is mixed this analysis still holds as explained in Ref. [18], because the corresponding volume fraction cancels out and the effect of mix modifying the electron density is negligible.

* bachmann2@llnl.gov

[1] A. B. Zylstra *et al.*, Burning plasma achieved in inertial fusion, Nature **601**, 542-548 (2022).

[2] H. Abu-Shawareb *et al.*, Lawson's criteria for ignition exceeded in an inertial fusion experiment, Phys. Rev. Lett. **129**, 075001 (2022).

[3] M. J. Edwards *et al.*, The experimental plan for cryogenic layered target implosions on the National Ignition Facility - The inertial confinement approach to fusion, Phys. Plasmas **18**, 051003 (2011).

[4] J. D. Lindl *et al.*, The physics basis for ignition using indirect-drive targets on the National Ignition Facility, Phys. Plasmas **11**, 339 (2004).

[5] J. D. Lindl, Development of the indirect-drive approach to inertial confinement fusion, and the target physics basis for ignition, and gain, Phys. Plasmas **2**, 3933 (1995).

[6] M. L. Spaeth *et al.*, Description of the NIF Laser, Fusion Sci. Technol. **59**, 25-145, (2016).

[7] A. B. Zylstra *et al.*, Record Energetics for an Inertial Fusion Implosion at NIF, Physical Review Letters **126**, 025001 (2021).

[8] O. Hurricane *et al.*, Approaching a burning plasma on the NIF, Physics of Plasmas **26**, 052704 (2019).

[9] A. B. Zylstra *et al.*, Hot-spot mix in large-scale HDC implosions at NIF, Phys. Plasmas **27**, 092709 (2020).

[10] D. S. Clark *et al.*, Capsule physics comparison of National Ignition Facility implosion designs using plastic, high density carbon, and beryllium ablators, Phys. Plasmas **25**, 032703 (2018).

[11] S.P. Regan *et al.*, Hot-spot mix in ignition-scale Inertial Confinement fusion targets, Phys. Rev. Lett. **111**, 045001 (2013).

[12] T. Ma *et al.*, Onset of Hydrodynamic Mix in High-Velocity, Highly Compressed Inertial Confinement Fusion Implosions, Phys. Rev. Lett. **111**, 085004 (2013).

[13] B. Bachmann *et al.*, Localized mix-induced radiative cooling in a capsule implosion at the National Ignition Facility, Physical Review E **101**, 033205 (2020).

[14] C. R. Weber *et al.*, Mixing in ICF implosions on the National Ignition Facility caused by the fill-tube, Physics of Plasmas **27**, 032703 (2020).

[15] A. Pak *et al.*, The impact of localized radiative loss on inertial confinement fusion implosions, Physical Review Letters **124**, 145001 (2020).

[16] J. E. Ralph *et al.*, Measurements of enhanced performance in an indirect drive inertial confinement fusion experiment when reducing the contact area of the capsule support, Physics of Plasmas **27**, 102708 (2020).

[17] V. A. Smalyuk *et al.*, Review of hydrodynamic instability experiments in inertially confined fusion implosions on National Ignition Facility, Plasma Physics and Controlled Fusion **62**, 014007 (2019).

[18] T. Ma *et al.*, The role of hot spot mix in the low-foot and high-foot implosions on the NIF, Phys. Plasmas **24**, 056311 (2017).

[19] K. L. Baker *et al.*, Hotspot parameter scaling with velocity and yield for high-adiabat layered implosions at the National Ignition Facility, Physical Review E **102**, 023210 (2020).

[20] S. A. MacLaren *et al.*, A near one-dimensional indirectly driven implosion at convergence ratio 30, Phys. Plasmas **25**, 056311 (2018).

[21] V. A. Smalyuk *et al.*, Measurements of an Ablator-Gas Atomic Mix in Indirectly Driven Implosions at the National Ignition Facility, Phys. Rev. Lett. **112**, 025002 (2014).

[22] O. L. Landen *et al.*, Yield and compression trends and reproducibility at NIF, High Energy Density Physics **36**, 100755 (2020).

[23] G. Zimmerman *et al.*, Numerical simulation of laser-initiated fusion, Comments Plasma Phys. Controlled Fusion **2**, 51–60 (1975).

[24] Y. Zhou *et al.*, Formulation of a two-scale transport scheme for the turbulent mix induced by Rayleigh-Taylor and Richtmyer-Meshkov instabilities, Physical Review E **65**, 056303 (2002).

[25] G. Dimonte, Spanwise homogeneous buoyancy-drag model for Rayleigh–Taylor mixing and experimental evaluation, Phys. Plasmas **7**, 2255 (2000).

[26] O. A. Hurricane, E. Burke, S. Maples and M. Viswanathan, Saturation of Richtmyer's impulsive model, Physics of Fluids **12**, 2148 (2000).

[27] H. F. Robey, Effects of viscosity and mass diffusion in hydrodynamically unstable plasma flows, Phys. Plasmas **11**, 4123 (2004)

[28] Y. Zhou, Unification and extension of the similarity scaling criteria and mixing transition for studying astrophysics using high energy density laboratory experiments or numerical simulations, Phys. Plasmas **14**, 082701 (2007))

[29] A. S. Moore *et al.*, The five line-of-sight neutron time-of-flight (nToF) suite on the National Ignition Facility (NIF), Rev. Sci. Instrum. **92**, 023516 (2021).

[30] L. C. Jarrott *et al.*, Thermal Temperature Measurements of Intertial Fusion Implosions, Phys. Rev. Lett. **121**,

085001 (2018).
[31] P. K. Patel *et al.*, Hotspot conditions achieved in inertial confinement fusion experiments on the National Ignition Facility, Phys. Plasmas **27**, 050901 (2020).
[32] D. T. Casey *et al.*, Development of the CD Symcap platform to study gas-shell mix in implosions at the National Ignition Facility, Phys. Plasmas **21**, 092705 (2014).
[33] B. Bachmann *et al.*, Resolving hot-spot microstructure using x-ray penumbral imaging (invited), Rev. Sci. Instrum. **87**, 11E201 (2016).
[34] F. Pérez *et al.*, The NIF x-ray spectrometer calibration campaign at Omega, Rev. Sci. Instrum. **85**, 11D613 (2014).
[35] C. Krauland *et al.*, Design of the National Ignition Facility Imaging and Spectroscopy Snout (ISS), APS Division of Plasma Physics Meeting (2019).
[36] D. H. Munro, Interpreting inertial fusion neutron spectra, Nucl. Fusion **56**, 036001 (2016).
[37] H. A. Scott and S. B. Hansen, Advances in NLTE modeling for integrated simulations, High Energy Density Phys. **6**, 39 (2010).